Article

Crystal Structures and Optical Properties of Two Novel 1,3,5-Trisubstituted Pyrazoline Derivatives

Qi Feng [1], Wenhui Huan [1], Jiali Wang [1], Jiadan Lu [1], Guowang Diao [1,*] and Yaqi Shan [2]

[1] School of Chemistry & Chemical Engineering, Yangzhou University, Yangzhou 225002, China; 006450@yzu.edu.cn (Q.F.); 18252722156@163.com (W.H.); jlwang0060@163.com (J.W.); 18762314798@163.com (J.L.)

[2] School of Chemistry and Chemical Engineering, Southeast University, Nanjing 211189, China; 230159523@seu.edu.cn

* Correspondence: gwdiao@yzu.edu.cn; Tel.: +86-0514-8797-5587

check for updates

Abstract: Two novel 1,3,5-trisubstituted pyrazoline derivatives—1-acetyl-3-(4-methoxyphenyl)-5-(6-methoxy-2-naphthyl)-pyrazoline (2a) and 1-(4-nitrophenyl)-3-(4-methoxyphenyl)-5-(6-methoxy-2-naphtyl)-pyrazoline (2b)—were synthesized and their structures were determined by single crystal X-ray crystallography. Both of the two crystals exhibit twisted structures due to the large dihedral angles between the pyrazolinyl ring and the aromatic ring at the 5-position (88.09° for 2a and 71.26° for 2b). The optical–physical properties of the two compounds were investigated. The fluorescent emission of 2b arises from the 1,3-disubstituted pyrazoline chromophores and exhibits a red shift in polar solvents and solid-state, which could be attributed to photo-induced intramolecular charge transfer (ICT) from N1 to C3 in the pyrazoline moiety and the intermolecular interactions within the crystal. The fluorescent emissions of 2a (λ_{max} 358–364 nm) in solvents and solid-state both come from 6-methoxy-2-naphthyl chromophores, which are fairly insensitive to the solvent polarity.

Keywords: pyrazoline derivatives; single crystal; fluorescence

1. Introduction

A development in the design and preparation of novel organic luminescent materials has recently been the subject of great interest from both academia and industry, including the fields of fluorescent biological labels, optical sensors, and organic light-emitting diodes (OLEDs) [1–4]. Amongst the numerous organic luminescent materials, pyrazoline and its derivatives have received increasing attention due to their excellent electro–optical properties and wide range of applications [5–10]. In the past decades, although extensive research has focused on the photophysical properties of 1,3,5-triaryl-substituted pyrazolines [11,12], 1-acetyl-pyrazoline derivatives have also attracted a lot of attention because they have many unique advantages [13]. For example, a large number of 1-acetyl-pyrazoline derivatives show high sensitivity and selectivity towards different metal ions and can be used as fluorescent sensors [14]. However, relevant research about the photophysical properties of 1-acetyl-pyrazoline derivatives, especially in solid-state, is rare.

In this work, two novel 1,3,5-trisubstituted pyrazoline derivatives: 1-acetyl-3-(4-methoxyphenyl)-5-(6-methoxy-2-naphthyl)-pyrazoline (2a) and 1-(4-nitrophenyl)-3-(4-methoxyphenyl)-5-(6-methoxy-2-naphtyl)-pyrazoline (2b) were synthesized and their structures were confirmed by X-ray crystallographic analyses. The two compounds contain the same substituent groups on 3- and 5-positions, but different electron-withdrawing groups on 1-position. According to previous reports, the substituent groups on 1-position of the pyrazoline ring could primarily influence the photophysical properties [15]. Thus, the different optical-physical

properties of the two compounds in solvents and solid-state were investigated and discussed. Moreover, from the view of crystallography, the introduction of the hydrogen bond acceptors, such as methoxyl and carbonyl groups, could cause the formation of hydrogen bonds, which may primarily affect their 3D crystal structures. Therefore, Hirshfeld surface analysis was also performed to give insight regarding intermolecular interactions in the two crystals.

2. Materials and Methods

2.1. Synthesis

The pyrazoline derivatives were synthesized by the following reactions (Scheme 1). Chalcones (1a and 1b) were synthesized by condensing 1-(4-methoxyphenyl)ethanone with aryl aldehyde in a dilute ethanolic sodium hydroxide solution at room temperature, according to the Claisen-Schmidt condensation given in the literature [16,17].
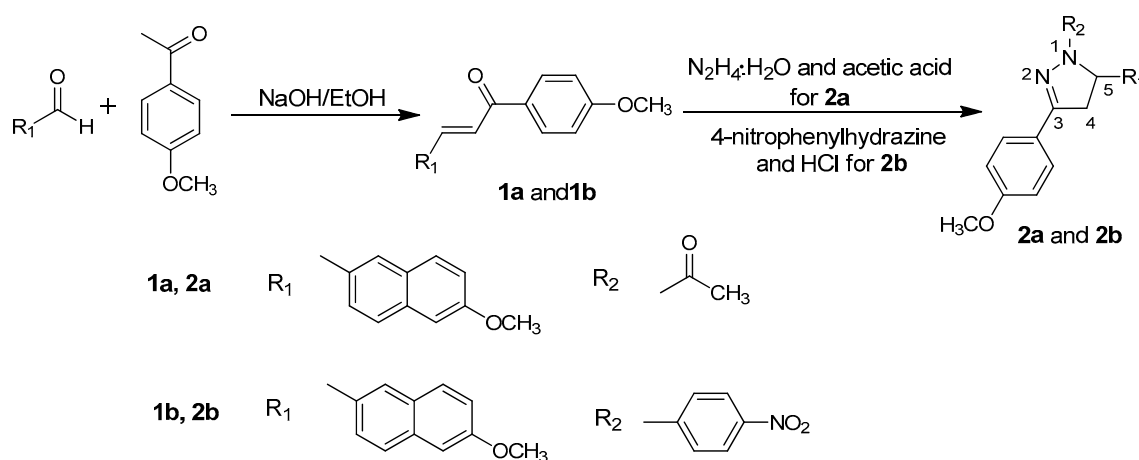
Scheme 1. Syntheses of 2a and 2b.

2.1.1. Synthesis of 2a

A mixture of chalcone 1a (1.2466 g) and hydrazine hydrate (85%, 2 mL) in glacial acetic acid (6 mL) was refluxed at 110 °C for 4 h. The reaction mixture was then poured into ice water. The crude product was filtered and recrystallized from ethyl acetate/petroleum ether (v/v = 2:1) to afford compound 2a in 91% yield as white crystals, m.p. 116–118 °C. ^{1}H Nuclear Magnetic Resonance (NMR) (300 MHz, CDCl$_3$, Figure S1) δ ppm: 2.43 (s, 3H), 3.16–3.23 (dd, 1H), 3.70–3.81 (m, 1H), 3.84–3.89 (d, 6H), 5.68–5.72 (dd, 1H), 6.92–7.71 (m, 10H). IR (KBr, cm^{-1}, Figure S2): 3450, 2946, 2302, 1653, 1606, 1516, 1444, 1409, 1248, 1176, 1030, 852, 626, 559.

2.1.2. Synthesis of 2b

A mixture of chalcone 1b (0.9978 g), 4-nitrophenylhydrazine (0.5401 g), and HCl (37%, 1 mL) in ethanol (10 mL) was refluxed for 8 h. The precipitate was filtered from the cool reaction solution and further recrystallized from ethyl acetate and petroleum ether (v/v = 3:1) to afford compound 2b in 83% yield as yellow crystals, m.p. 214–216 °C. ^{1}H NMR (300 MHz, CDCl$_3$, Figure S3) δ ppm: 3.24–3.32 (dd, 1H), 3.85–3.90 (m, 6H), 3.95–4.00 (m, 1H), 5.48–5.54 (dd, 1H), 6.93–8.04 (m, 14H). IR (KBr, cm^{-1}, Figure S4): 3444, 1593, 1494, 1400, 1305, 1250, 1172, 1109, 1026, 839, 680.

2.2. Crystals' Preparation

The single crystals of the two compounds were recrystallized in ethanol. Slow evaporation of the solvents at room temperature for 4–5 days yielded colorless (2a) and yellow (2b) prism crystals.

2.3. Measurement

The ^{1}H NMR spectra were recorded at 297 K on a Bruker Avance 300 MHz NMR spectrometer (Bruker, Billerica, MA, USA) using $CDCl_3$ as solvent and Tetramethyl silane (TMS) as internal standard. The IR spectra were measured on a Bruker Tensor 27 FT-IR spectrometer (Bruker, Billerica, MA, USA) with KBr pellets in the range 4000–400 cm^{-1}. UV-Vis absorption spectra were recorded on a Shimadzu UV-2450 spectrometer (Shimadzu, Kyoto, Japan) operating between 190 and 900 nm. Fluorescence spectra were obtained with a Horiba FluoroMax 4 spectrofluorometer (HORIBA Scientific, Kyoto, Japan).

Single X-ray diffraction data for the two crystals were collected on a Rigaku SCXmini diffractometer (Rigaku, Tokyo, Japan) with a Mercury2 CCD area-detector by using graphite-monochromatized Mo-Kα radiation (λ = 0.71073 Å). The structures were solved with direct methods using the SHELXS-97 program (University of Göttingen, Göttingen, Germany, 1997) and refined anisotropically with SHELXTL-97 using full-matrix least-squares procedure [18]. All non-hydrogen atoms were refined with anisotropic displacement parameters and were placed in idealized positions. The structural data for three crystals have been deposited as CIFs at the Cambridge Crystallographic Data Base (CCDC No. 911423 and 911424) and are also available as Supporting Information (SI). Powder X-ray diffraction (PXRD) patterns were measured with a Bruker D8 advance superspeed powder diffractometer, which operated at ambient temperature, using Cu Kα radiation (λ = 0.15405 nm).

2.4. Hirshfeld Surface Analysis

Hirshfeld surface analysis was performed by using Crystal Explorer 3.1(University of Western Australia: Perth, Australia, 2012) [19].

3. Results

3.1. Crystal Structure

Single crystal X-ray diffraction analyses were performed for the two crystals to determine their structures. A summary of the crystallographic data are shown in Table 1, and selected bond distance and angle are shown in Table 2. From the thermal ellipsoid plots (Figure 1), each asymmetric unit (ASU) accommodates only one molecule, and both of them exhibited twisted structures with dihedral angles between the pyrazolinyl ring and the aromatic ring at the 5-position of 88.09° (2a) and 71.26° (2b), respectively. However, the other aromatic rings at 1- or 3-positions were almost coplanar with the pyrazoline rings, and the dihedral angles are 4.61° for 2a and 4.61° and 5.47° for 2b. In the two crystals, N1–N2 bond length was shorter than the typical N–N single bond (1.45 Å) and longer than the typical N=N bond (1.25 Å), and the N2=C3 bond length was shorter than the typical N=C double bond (1.35 Å). These coplanar structures and the shorter bond lengths suggested the formation of a conjugated π system in the two molecules, which were composed of N1, N2, C3 atoms in pyrazoline ring and the substituents at 1- and 3-positions.

Table 1. Crystallographic data and refinement for 2a and 2b.

Crystal	2a	2b
Molecular formula	$C_{23}H_{22}N_2O_3$	$C_{27}H_{23}N_3O_4$
Formula weight	374.43	452.48
Crystal system	Monoclinic	Monoclinic
Space group	$P2_1/n$	$P2_1/c$
a (Å)	8.5757 (17)	10.356 (2)
b (Å)	17.422 (4)	20.342 (4)
c (Å)	13.279 (3)	11.787 (2)
α (°)	90.00	90.00
β (°)	97.65 (3)	112.81 (3)
γ (°)	90.00	90.00 (3)
volume (Å^3)	1966.3 (7)	2288.7 (8)
density (g/cm^3)	1.265	1.316
Z	4	4
$F(000)$	792	952
Absorption coefficient/mm^{-1}	0.084	0.090
Parameters	256	309
θ Range for data collection/°	3.02–27.48	3.00–25.00
R_1 ($I > 2\sigma(I)$)	0.0726	0.0856
w R_2 ($I > 2\sigma(I)$)	0.1569	0.1655
GOF	1.024	1.016
CCDC No.	911423	911424

Table 2. Selected bond lengths (Å) and angles (°) for the two crystals.

Parameter	2a	2b
N1–N2	1.396	1.407
N1–C2	1.362	1.380
N1–C5	1.483	1.479
N2–C3	1.293	1.299
C3–C6	1.460	1.461
C3–C4	1.507	1.501
C4–C5	1.539	1.540
C5–C13	1.510	1.515
N2–C3–C6 (degree)	122.1	122.5
C2–N1–N2 (degree)	121.9	117.5
N1–C5–C13 (degree)	111.0	115.6
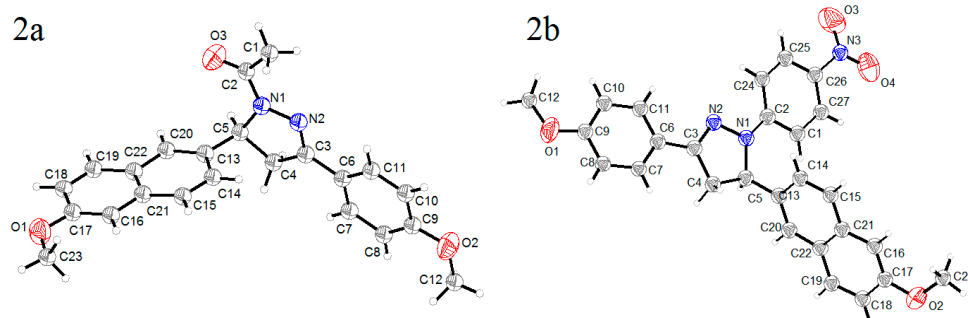
Figure 1. Thermal ellipsoids plots of crystals 2a and 2b at 20% probability.

It can be seen that 2a crystallizes in space group $P2_1/n$. As shown in Figure 2, the two neighboring heterochiral molecules are connected via weak C–H···O hydrogen bonds (Table 3) to afford the racemic dimer. The dimers also associate through weak C–H···O hydrogen bonds along the *a* axis to form the racemic chain motifs, which are connected with each other to provide its 3D structure. Moreover, the

closest centroid distance between adjacent naphthalene rings is 5.382 Å, indicating that there is no strong π-overlap between them.
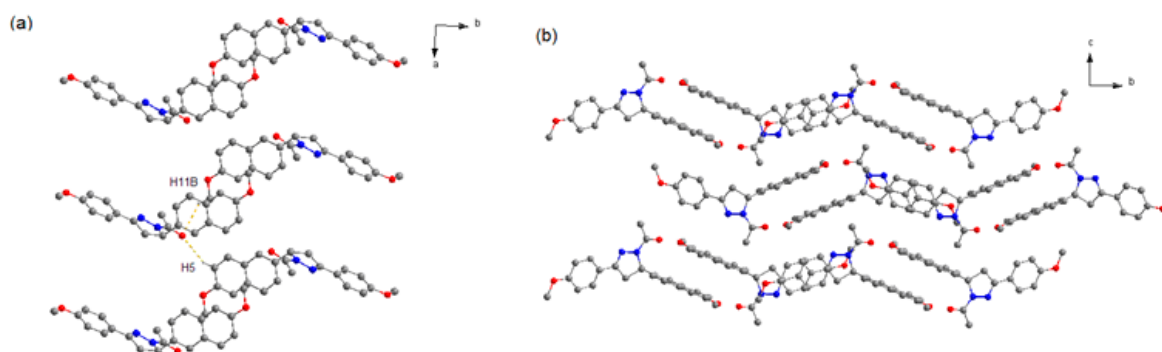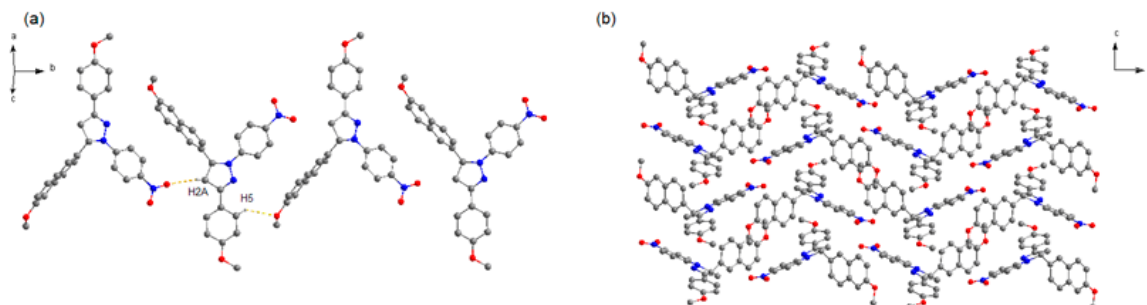

Figure 2. Crystal structure of 2a (**a**) Racemic chain motif. (**b**) 3D packing diagram of crystal 2a (projected in *bc* plane). The dotted lines show the weak hydrogen bonds. C atoms in gray, N atoms in blue, and O atoms in red. H atoms not participating in the interactions have been omitted for clarity.

Table 3. Intermolecular weak C–H⋯O hydrogen bond parameters in the two crystals.

| Crystal	D–H (Å)	H⋯A (Å)	D⋯A (Å)	D–H⋯A (°)
2a				
C14–H1⋯O2	0.930	2.453	3.178	134.93
C18–H5⋯O3	0.929	2.527	3.378	152.42
C12–H21B⋯O1	0.960	2.566	3.503	165.36
C23–H11B⋯O3	0.960	2.699	3.438	134.18
C7–H16⋯O1	0.929	2.603	3.458	153.09
2b				
C11–H5⋯O2	0.930	2.710	3.393	130.97
C4–H2A⋯O3	0.970	2.521	3.133	120.97
C18–H14⋯O4	0.931	2.526	3.370	150.73

It can be seen that 2b crystallizes in space group $P2_1/c$. In this structure (Figure 3), the one-handed enantiomers associate along the *b* axis to construct two kinds of homochiral chain motifs. The two homochiral chains with mirror symmetry are stacked alternately along the *c* axis to form the 2D structure, which are stacked in a parallel fashion to give the 3D crystal structure. Like crystal 2a, no strong π–π interaction exists between adjacent naphthalene rings, due to the long distance of 5.469 Å between the two centroids.

Figure 3. Crystal structure of 2b. (**a**) Homochiral chain motif. (**b**) 3D packing diagram of crystal 2b (projected in *bc* plane). The dotted lines show the weak hydrogen bonds. C atoms in gray, N atoms in blue, and O atoms in red. H atoms not participating in the interactions have been omitted for clarity.

3.2. Hirshfeld Surface Analyses

Both compounds 2a and 2b contain several hydrogen bond acceptors, such as methoxyl, carbonyl, and nitryl groups. Hirshfeld surface analysis was performed to give insight regarding the intermolecular interactions in the two crystals [20]. The inspection of the intermolecular interactions was normalized by van der Waals radii through a red-white-blue color scheme, where the red spots denote closer contacts. From the Hirshfeld surface (Figure 4), several red spots were obviously observed on oxygen atoms on carbonyl and two methoxyl groups of 2a and oxygen atoms on nitryl groups of 2b, corresponding to the weak C–H···O hydrogen bonds. Moreover, all the other red spots exist around H atoms, and most of them are also attributed to the weak C–H···O hydrogen bonds. That is to say, due to the introduction of the hydrogen bond acceptors, these weak hydrogen bonds play a key role in crystal packing for the two crystals.
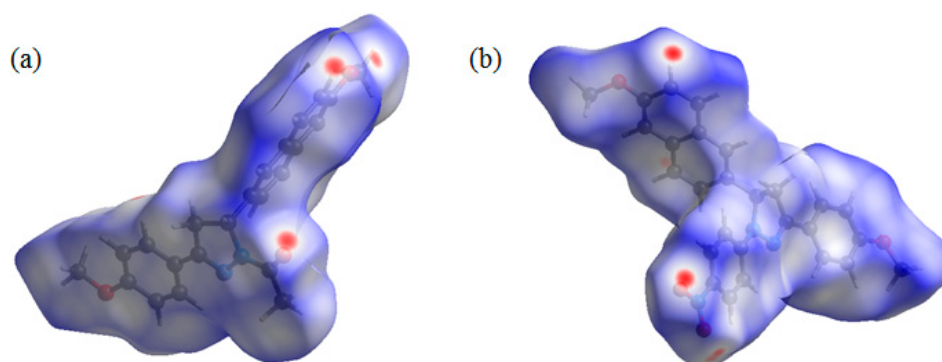
Figure 4. Hirshfeld surface mapped with d_{norm} for the molecules of 2a (**a**) and 2b (**b**).

A two-dimensional fingerprint plot over the Hirshfeld surface was used to highlight the contribution of the intermolecular interactions for crystal packing (Figure 5 and Table 4). It was found that weak H···H contacts made the major contribution in the two crystals, with 51.5% and 39.9% of total surface area, respectively. The C···H contacts were second largest contribution, comprising 25.5% and 31.5% of total surface area, respectively. Apart from that, O···H contacts caused by weak C–H···O hydrogen bonds also showed important contribution for the supramolecular architectures with 17.3% and 22.2% of total surface area, respectively, which appear as two wings in the left (H···O) and right (O···H) areas of the related plots (Figure S5).
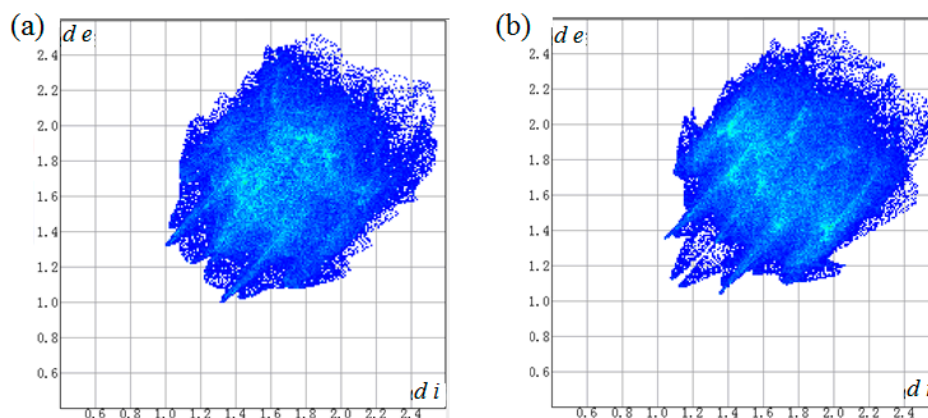

Figure 5. Two-dimensional fingerprint plots for the molecules of 2a (**a**) and 2b (**b**).

Table 4. Contributions of the intermolecular contacts.

Crystal	H···H %	C···H %	O···H %	N···H %	C···C %	C···O %	C···N %	O···N %	O···O %
2a	39.9	31.5	22.2	3.2	0.5	0.6	1.7	0.3	0.2
2b	51.5	25.5	17.3	2.6	2.7	0.2	0.1	0	0

3.3. Photo-Physical Properties

The absorption spectra of the two compounds in different solvents are shown in Figure 6. Because naphthalene exhibits several maximum peaks near 350 nm, the absorption of 2a was considered a combination of 1-acetyl-3-(4-methoxyphenyl)-pyrazolinyl and the 6-methoxy-2-naphthyl chromophores. In addition, it could be observed that the absorption spectra of 2a exhibit little change with increasing solvent polarity, indicating that there is no charge transfer in its ground state. Compound 2b exhibits two absorption bands around 400 nm in non-polar solvent n-hexane (Table 5), which should be ascribed to the π–π* transition of the 3-(4-methoxyphenyl)-1-(4-nitrophenyl)-2-pyrazoline chromophore. Compared with other 1,3,5-triphenyl-pyrazoline and 1,3-diphenyl-pyrazolines, the absorption band shifts to lower energy in the solvents of moderate polarity. The red shift may be attributed to the stronger electron-withdrawing group located in 1-position in 2b, which causes an intramolecular charge transfer (CT) character for the transition.
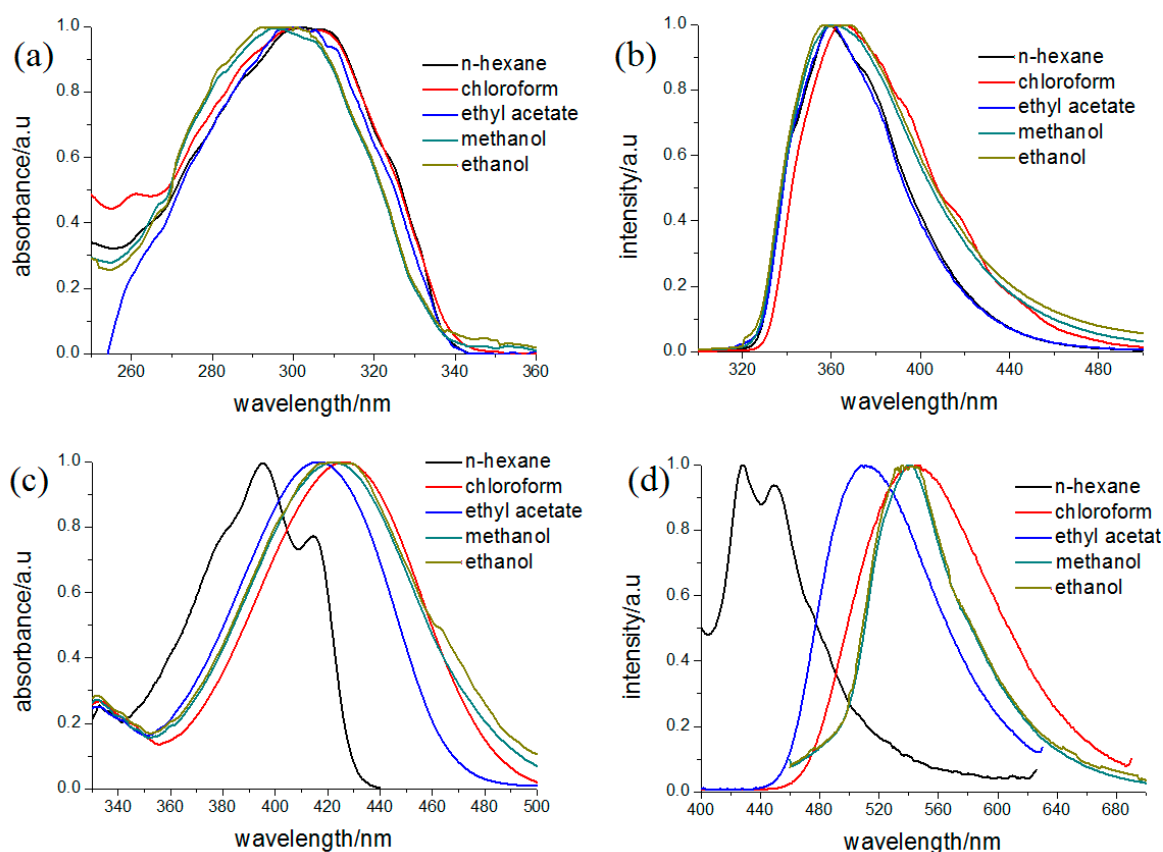

Figure 6. Absorption and fluorescence spectra of 2a (**a,b**) and 2b (**c,d**) in various solvents (10^{-4} mol/L).

Table 5. Spectroscopic data of 2a and 2b.

Solvents	2a		2b	
	λ_{ab} (nm)	λ_{em} (nm)	λ_{ab} (nm)	λ_{em} (nm)
n-Hexane	302	358	395	428
Chloroform	300	364	426	547
Ethyl acetate	300	359	416	508
Ethanol	294	358	422	533
Methanol	294	360	422	540

Corresponding to the absorption spectra, the fluorescent spectra of 2b also exhibits a large red shift in the polar solvents. When the solvent is changed from n-hexane to methanol, the red shift in their emission bands is nearly 110 nm. The red shift could be attributed to an intramolecular charge transfer (ICT) state formed by intramolecular electron transfer in the 3-(4-methoxyphenyl)-1-(4-nitrophenyl)-2-pyrazoline chromophore, which is effectively stabilized in polar media such as methanol and causes an increase of Stokes' shift. These characters are similar with 5-(9-anthryl)-3-(4-nitrophenyl)-1-phenyl-2-pyrazoline (ANPP) [21,22]. Although the nitro group exists on 3-position, it emitted a large red shift of about 110 nm in the polar solvents, which is also caused by charge transfer from N1 to C3 in the pyrazoline moiety in the excited state. In contrast, 2a exhibited only one band with fluorescence maxima centered at 358 nm in the n-hexane and no obvious change could be found with increasing the polarity of solvents. It was considered that the fluorescence of 2a arises from the 6-methoxy-2-naphthyl, and the fluorescence of pyrazoline is quenched due to the enhanced intersystem crossing from the pyrazoline excited state [23]. Similar circumstances could be found in 1-acetyl-3-naphthyl-5-(9-anthryl)-2-pyrazoline (APPP), where the emission band is assigned to anthracene chromophore and is fairly insensitive to the solvent polarity [24], suggesting the same optical–physical process for these 1-acetyl-pyrazolines.

Solid fluorescence spectra of the two crystals are shown in Figure 7. The fluorescence spectrum of 2a is similar with that of ethanol, which exhibits two emission peaks at 360 and 374 nm. According to its crystal structure, no strong π–π interaction existed between naphthalene rings, so it was considered that the fluorescent emission of 2a should be attributed to monomer fluorescence of 6-methoxy-2-naphthyl chromophore. Emission peaks of 2b are centered at 556 nm. Compared to its emission in the ethanol solvent, it had a red shift of 23 nm in solid state. In solid-state, the molecules are closer to each other, which result in enhancement of dipole-dipole interaction of the polarized excited-state and a larger red shift in its fluorescence spectrum.
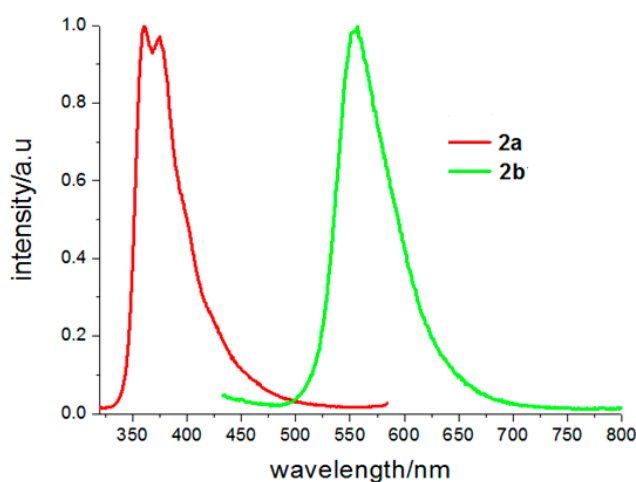
Figure 7. Solid fluorescence spectra of 2a and 2b (the fluorescence emission spectra excited at 300 nm for 2a and 400 nm for 2b).

4. Conclusions

In summary, two novel 1,3,5-trisubstituted pyrazoline derivatives were synthesized and their structures were confirmed by IR, ^{1}H NMR and X-ray crystallographic analysis. It was found that the aromatic rings at 5-position are almost perpendicular with pyrazoline rings, while the aromatic rings at 1- and 3-position pyrazoline rings are nearly coplanar to form the conjugated π-system. According to Hirshfeld Surface analysis, due to the introduction of hydrogen bond acceptors, the weak C–H···O hydrogen bonds play a key role in crystal packing for the two crystals. Fluorescence measurement revealed the primary influence of the substituent groups on 1-position of pyrazoline ring. For 2b, the emission arises from the 1,3-disubstituted pyrazoline chromophores and the mechanism involves photo-induced intramolecular charge transfer (ICT) from N1 to C3 in the pyrazoline moiety. The fluorescent emission of 2a comes from the 6-methoxy-2-naphthyl chromophore, which shows little change when increasing the polarity of solvents.

Supplementary Materials: The following are available online at http://www.mdpi.com/2073-4352/8/12/467/s1, X-ray crystallographic information files (CIF) for the two crystals.

Author Contributions: Q.F. designed the experiments and wrote and revised the manuscript. W.H. and J.W. performed the X-ray single diffraction study and Hirshfeld surface analyses. J.L. performed ^{1}H NMR and IR spectra spectroscopy. Y.S. synthesized the compounds and crystals. G.D. conceived the project.

Conflicts of Interest: The authors declare no conflict of interest.

References

1. Lustig, W.P.; Mukherjee, S.; Rudd, N.D.; Desai, A.V.; Li, J.; Ghosh, S.K. Metal-organic frameworks: Functional luminescent and photonic materials for sensing applications. *Chem. Soc. Rev.* **2017**, *46*, 3242–3285. [CrossRef]

2. Gong, X.Q.; Cai, J.; Zhang, B.; Zhao, Q.; Piao, J.F.; Peng, W.P.; Gao, W.C.; Zhou, D.M.; Zhao, M.; Chang, J. A review of fluorescent signal-based lateral flow immunochromatographic strips. *J. Mater. Chem. B* **2017**, *5*, 5079–5091. [CrossRef]

3. Wu, A.L.; Sun, P.P.; Sun, N.; Yu, Y.; Zheng, L.Q. Coassembly of a Polyoxometalate and a Zwitterionic Amphiphile into a Luminescent Hydrogel with Excellent Stimuli Responsiveness. *Chem.-Eur. J.* **2018**, *24*, 16857–16864. [CrossRef] [PubMed]

4. Bui, T.T.; Goubard, F.; Ibrahim-Ouali, M.; Gigmes, D.; Dumur, F. Recent advances on organic blue thermally activated delayed fluorescence (TADF) emitters for organic light-emitting diodes (OLEDs). *Beilstein. J. Org. Chem.* **2018**, *14*, 282–308. [CrossRef] [PubMed]

5. Zhang, L.; Liu, J.; Gao, J.K.; Zhang, F.; Ding, L. High Solid Fluorescence of a Pyrazoline Derivative through Hydrogen Bonding. *Molecules* **2017**, *22*, 1304. [CrossRef] [PubMed]

6. Varghese, B.; Al-Busafi, S.N.; Suliman, F.O.; Al-Kindy, S.M.Z. Unveiling a versatile heterocycle: Pyrazoline a review. *RSC Adv.* **2017**, *7*, 46999–47016. [CrossRef]

7. Haupa, K.A.; Szukalski, A.; Mysliwiec, J. Low-Molecular Push Pull Pyrazoline Derivatives: Solvatochromic Effect and Theoretical Insights into Dye-based Molecular Engineering. *J. Chem. Phys.* **2018**, *122*, 7808–7818. [CrossRef] [PubMed]

8. Vandana, T.; Ramkumar, V.; Kannan, P. Synthesis and fluorescent properties of poly(arylpyrazoline)'s for organic-electronics. *Opt. Mater.* **2016**, *58*, 514–523. [CrossRef]

9. Zhang, R.-R.; Zhang, J.-F.; Wang, S.-Q.; Cheng, Y.-L.; Miao, J.-Y.; Zhao, B.-X. Novel pyrazoline-based fluorescent probe for detecting thiols and its application in cells. *Spectrochim. Acta. A* **2015**, *137*, 450–455. [CrossRef]

10. Singh, P.; Rawat, B.; Rawat, B.S.; Pant, G.J.N.; Rawat, M.S.M.; Joshi, G.C. Synthesis, centrifugal chromatographic separation and fluorescence study of a 2-pyrazoline. *J. Indian Chem. Soc.* **2014**, *91*, 1555–1559.

11. Jin, M.; Liang, Y.J.; Lu, R.; Chuai, X.H.; Yi, Z.H.; Zhao, Y.Y.; Hong, J.Z. Synthesis and properties of photoluminescence and electroluminescence of pyrazoline derivatives. *Synth. Met.* **2004**, *140*, 37–41. [CrossRef]

12. Bai, G.; Li, J.F.; Li, D.X.; Dong, C.; Han, X.Y.; Lin, P.H. Synthesis and spectrum characteristic of four new organic fluorescent dyes of pyrazoline compounds. *Dyes Pigment.* **2007**, *75*, 93–98. [CrossRef]

13. Maslakci, N.N.; Eren, E.; Topel, S.D.; Cin, G.T.; Oksuz, A.U. Electrospun plasma-modified chitosan/poly(ethylene terephthalate)/ferrocenyl-substituted N-acetyl-2-pyrazoline fibers for phosphate anion sensing. *J. Appl. Polym. Sci.* **2016**, *133*, 43344. [CrossRef]

14. Yang, A.B.; Xu, Z.X.; Wu, J.; Feng, Y.Y.; Wang, B.X. Synthesis of 1-Acetyl-3-(2-hydroxyl-4,6-dimethoxylphenyl)-5-phenyl-2-pyrazoline and Studies on Its Zinc Ion Probe. *Chem. J. Chin. Univ.* **2010**, *31*, 1365–1368.

15. Fahrni, C.J.; Yang, L.C.; VanDerveer, D.G. Tuning the photoinduced electron-transfer thermodynamics in 1,3,5-triaryl-2-pyrazoline fluorophores: X-ray structures, photophysical characterization, computational analysis, and in vivo evaluation. *J. Am. Chem. Soc.* **2003**, *125*, 3799–3812. [CrossRef] [PubMed]

16. Ohashi, K.; Kinoshita, Y.; Tamiaki, H. Synthesis of chlorophyll-a derivatives possessing the 3-(2-acylethenyl) group by cross-aldol condensation and their optical properties. *Tetrahedron* **2018**, *74*, 2703–2715. [CrossRef]

17. Mellado, M.; Madrid, A.; Martinez, U.; Mella, J.; Salas, C.O.; Cuellar, M. Hansch's analysis application to chalcone synthesis by Claisen-Schmidt reaction based in DFT methodology. *Chem. Pap.* **2018**, *72*, 703–709. [CrossRef]

18. Sheldrick, G.M. A short history of SHELX. *Acta Crystallogr. Sect. A Found. Crystallogr.* **2008**, *64*, 112–122. [CrossRef]

19. Wolff, S.K.; Grimwood, D.J.; McKinnon, J.J.; Jayatilaka, D.; Spackman, M.A. *CrystalExplorer 3.1*; The University of Western Australia: Perth, Australia, 2012.

20. McKinnon, J.J.; Spackman, M.A.; Mitchell, A.S. Novel tools for visualizing and exploring intermolecular interactions in molecular crystals. *Acta Crystallogr. Sect. B Struct. Sci.* **2004**, *60*, 627–668. [CrossRef]

21. Bozkurt, E.; Gul, H.I.; Mete, E. Solvent and substituent effect on the photophysical properties of pyrazoline derivatives: A spectroscopic study. *J. Photoch. Photobio. A* **2018**, *72*, 703–709. [CrossRef]

22. Wang, M.L.; Zhang, J.X.; Liu, J.Z.; Xu, C.X.; Ju, H.X. Intramolecular energy and charge transfer in 5-(9-anthryl)-3-(4-nitrophenyl)-1-phenyl-2-pyrazoline. *J. Lumin.* **2002**, *99*, 79–83. [CrossRef]

23. Kucukoz, B.; Sevinc, G.; Yildiz, E.; Karatay, A.; Zhong, F.; Yilmaz, H.; Tutel, Y.; Hayvali, M.; Zhao, J.; Yaglioglu, H.G. Enhancement of two photon absorption properties and intersystem crossing by charge transfer in pentaaryl boron-dipyrromethene (BODIPY) derivatives. *Phys. Chem. Chem. Phys.* **2016**, *18*, 13546–13553. [CrossRef] [PubMed]

24. Khan, A.; Wang, M.L.; Usman, R.; Lu, J.; Sun, H.; Du, M.; Zhang, R.M.; Xu, C.X. Organic charge-transfer complexes for the selective accommodation of aromatic isomers using anthracene derivatives and TCNQ. *New J. Chem.* **2016**, *40*, 5277–5284. [CrossRef]